

Possibilities for serial femtosecond crystallography sample delivery at future light sourcesa)

L. M. G. Chavas, L. Gumprecht, and H. N. Chapman

Citation: [Structural Dynamics](#) **2**, 041709 (2015); doi: 10.1063/1.4921220

View online: <http://dx.doi.org/10.1063/1.4921220>

View Table of Contents: <http://scitation.aip.org/content/aca/journal/sdy/2/4?ver=pdfcov>

Published by the [American Crystallographic Association, Inc.](#)

Articles you may be interested in

[Ceramic micro-injection molded nozzles for serial femtosecond crystallography sample delivery](#)

Rev. Sci. Instrum. **86**, 125104 (2015); 10.1063/1.4936843

[Serial femtosecond X-ray diffraction of enveloped virus microcrystals](#)

Struct. Dyn. **2**, 041720 (2015); 10.1063/1.4929410

[Time-resolved structural studies with serial crystallography: A new light on retinal proteins](#)

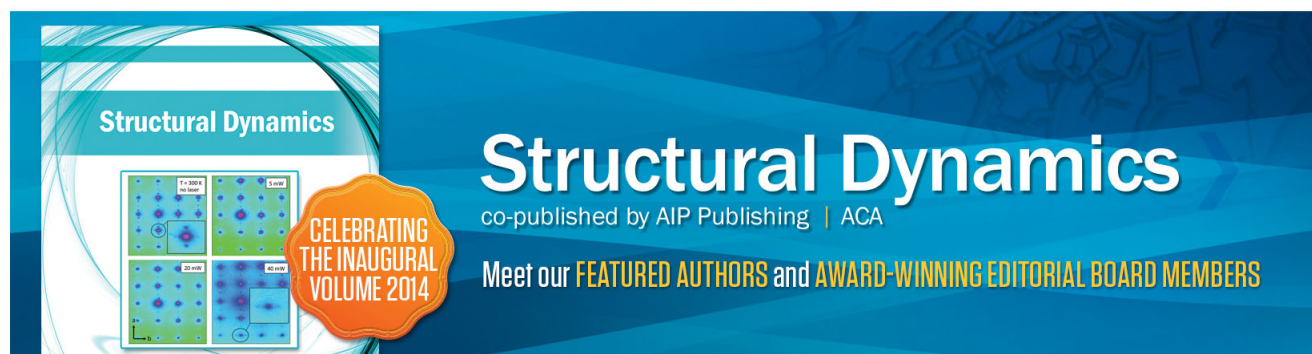
Struct. Dyn. **2**, 041718 (2015); 10.1063/1.4922774

[A split-beam probe-pump-probe scheme for femtosecond time resolved protein X-ray crystallography](#)

Struct. Dyn. **2**, 014102 (2015); 10.1063/1.4906354

[Investigations of amplitude and phase excitation profiles in femtosecond coherence spectroscopy](#)

J. Chem. Phys. **114**, 701 (2001); 10.1063/1.1329640



Structural Dynamics
co-published by AIP Publishing | ACA

CELEBRATING
THE INAUGURAL
VOLUME 2014

Meet our **FEATURED AUTHORS** and **AWARD-WINNING EDITORIAL BOARD MEMBERS**

Possibilities for serial femtosecond crystallography sample delivery at future light sources^{a)}

L. M. G. Chavas,^{1,b)} L. Gumprecht,¹ and H. N. Chapman^{1,2,3,b)}

¹Center for Free-Electron Laser Science, DESY, Notkestraße 85, 22607 Hamburg, Germany

²Department of Physics, University of Hamburg, Luruper Chaussee 149, 22607 Hamburg, Germany

³Centre for Ultrafast Imaging, Luruper Chaussee 149, 22607 Hamburg, Germany

(Received 24 March 2015; accepted 6 May 2015; published online 14 May 2015)

Serial femtosecond crystallography (SFX) uses X-ray pulses from free-electron laser (FEL) sources that can outrun radiation damage and thereby overcome long-standing limits in the structure determination of macromolecular crystals. Intense X-ray FEL pulses of sufficiently short duration allow the collection of damage-free data at room temperature and give the opportunity to study irreversible time-resolved events. SFX may open the way to determine the structure of biological molecules that fail to crystallize readily into large well-diffracting crystals. Taking advantage of FELs with high pulse repetition rates could lead to short measurement times of just minutes. Automated delivery of sample suspensions for SFX experiments could potentially give rise to a much higher rate of obtaining complete measurements than at today's third generation synchrotron radiation facilities, as no crystal alignment or complex robotic motions are required. This capability will also open up extensive time-resolved structural studies. New challenges arise from the resulting high rate of data collection, and in providing reliable sample delivery. Various developments for fully automated high-throughput SFX experiments are being considered for evaluation, including new implementations for a reliable yet flexible sample environment setup. Here, we review the different methods developed so far that best achieve sample delivery for X-ray FEL experiments and present some considerations towards the goal of high-throughput structure determination with X-ray FELs. © 2015 Author(s). All article content, except where otherwise noted, is licensed under a Creative Commons Attribution 3.0 Unported License.

[<http://dx.doi.org/10.1063/1.4921220>]

I. INTRODUCTION

The vast majority of high-resolution structures of macromolecules and macromolecular complexes have been determined by X-ray crystallography. All imaging methods that can attain molecular resolution use radiation that is energetic enough to ionize the sample, and with sufficient ionization events per given number of atoms (i.e., dose) the radiation can significantly degrade the structure under investigation. This problem of radiation damage can be overcome in X-ray crystallography by using well-ordered protein crystals with volumes greater than $1000\ \mu\text{m}^3$, allowing the measurement of diffraction intensities within a tolerable dose of about 30 MGy when the sample is cooled to cryogenic temperatures (Henderson, 1990 and Owen *et al.*, 2006). However, producing such large crystals is often not possible. Recently, a new approach to protein crystallography was demonstrated at X-ray free-electron laser (FEL) sources

^{a)}Contributed paper, published as part of the 2nd International BioXFEL Conference, Ponce, Puerto Rico, January 2015.

^{b)}Authors to whom correspondence should be addressed. Electronic addresses: leonard.chavas@desy.de and henry.chapman@desy.de.



that vastly increases the tolerable dose. Sufficiently short femtosecond-duration pulses from an X-ray FEL can give rise to the formation of diffraction patterns before the onset of radiation damage (Neutze *et al.*, 2000; Chapman *et al.*, 2011; and Spence and Chapman, 2014). This technique, called serial femtosecond crystallography (SFX), consists of recording thousands to millions of single-crystal single-pulse diffraction patterns. Since the first SFX experiments (Chapman *et al.*, 2011 and Boutet *et al.*, 2012), the technique has been refined and successfully applied to various biological systems including *in vivo* grown crystals (Redecke *et al.*, 2013), membrane proteins (Liu *et al.*, 2013), and photo-induced samples (Tenboer *et al.*, 2014). Phasing SFX data by anomalous diffraction have been demonstrated (Barends *et al.*, 2014).

The method of dispensing sample to the X-ray FEL beam depends on the size and quality of crystals available. For large crystals, a defocused pulse that imparts a dose of about 10 MGy creates a zone of destruction of approximately 25 μm diameter, and thus it is possible to collect short rotation series on a large frozen crystal by taking steps with larger spacing for each shot and rotation angle (Hirata *et al.*, 2014). With large crystals, it is possible to obtain strong diffraction with a beam attenuated to levels where the crystal can survive several shots. Such an approach could be used for time-resolved structural studies if the dose is kept below conventional levels (radiochemical processes will develop during the dark time between shots, and cryogenic cooling will confer the same benefit as for measurements with synchrotron radiation). Although the relationship between beam size, dose, and the range of destruction has not been systematically studied, one can surmise that protein crystals smaller than about 50 μm diameter can only be measured with a single destructive pulse to outrun radiation damage.

Various approaches have been developed and tried to deliver large numbers of small crystals of micrometer size or smaller to the beam, for the purpose of measuring a single diffraction pattern per shot. Under these conditions, there is no need to cryogenically cool the sample when using femtosecond X-ray pulses; samples can be measured at room temperature. The pulse vaporizes the exposed crystal, so data must be collected from a fresh crystal on each shot, and each exposure only gives a still diffraction pattern. A complete set of diffraction intensities can be acquired by collecting patterns in a serial fashion from a flowing sample, in which case each diffraction pattern is recorded at a random and unknown orientation of the crystal. This process is akin to powder diffraction. Indeed, if all patterns are summed together, a two-dimensional powder diffraction pattern is obtained. However, since the data are collected one grain at a time, it is possible to index each pattern and perform the summation on reflections of like Miller indices. In this way, a set of three-dimensional structure factors are obtained, where each is averaged over the same set of crystal shapes and sizes and beam fluctuations that would have produced a (non-overlapping) Debye-Scherrer ring. This analysis method is referred to as Monte Carlo integration (Kirian *et al.*, 2011; White *et al.*, 2012; and White *et al.*, 2013).

Various sample delivery systems have been implemented for experiments at the Linac Coherent Light Source (LCLS) in California and the SPring-8 Angstrom Compact free-electron LAsER (SACLA) in Japan. The two main classes of methods that have been demonstrated so far are flowing suspensions of crystals in a liquid or viscous medium across the beam and substrates or membranes supporting crystals that are rastered across the beam. With small or weakly diffracting crystals, it is crucial to keep the thickness of the supporting substrate or carrying medium to values that are not considerably larger than the crystals themselves, so that high-resolution reflections may be measured above the background generated by the medium. The first experiments at LCLS utilized gas-focused liquid jets (DePonte *et al.*, 2008) of sub-micron crystals suspended in their buffer solution. These jets are typically 1 to 5 μm in diameter. A nozzle that extrudes a viscous medium such as lipidic cubic phase (LCP) has also been successfully used to deliver to the beam membrane proteins that crystallize in that medium (Weierstall *et al.*, 2014). While producing higher background than liquid jets, the membrane crystals studied so far in LCP tended to be larger than 10 μm in diameter. The low flow rate of the LCP jet gives rise to about a 20-fold reduction in sample consumption for the same number of patterns collected with liquid jets. A low-flow extrusion of a grease matrix has also been tried (Sugahara *et al.*, 2015). Electrospinning jets have lower flow rates than liquid jets and also consume less material compared with gas-focused liquid jets (Sierra *et al.*, 2012). While

not yet tested extensively with crystals, aerosol beams created using aerodynamic lenses (Liu *et al.*, 1995) have been used to collect coherent diffraction patterns from non-crystalline samples such as nanoparticles (Bogan *et al.*, 2008), soot (Loh *et al.*, 2012), cell organelles (van der Schot *et al.*, 2015), and viruses (Seibert *et al.*, 2011). A new innovation of a compact aerosol injector with improved particle focusing is described by Kirian *et al.* (2015).

There are many ways to design experiments, and the field is still young and evolving. It is helpful to consider the priorities of an experimental design for serial crystallography, which are to (1) maximize diffraction data quality, especially on small samples; (2) maximize diffraction data collected per quantity of sample; and (3) maximize the experimental capacity by minimizing time for data collection and any down time. Since these guiding principles can in some situations be contradictory, or be quite dependent on the sample properties, a prudent design would maximize the diversity of data collection techniques and ideally be flexible enough to accommodate new improvements.

While many groups are steadily improving the reliability of various delivery systems, and introducing new innovations, experiments often have to contend with jets that vary in direction or other jetting properties with time, and with wide ranges of the composition and viscosity of the jet medium. These problems often lead to loss of measurement time, as the injection system needs to be replaced and re-aligned.

We review here different sample delivery methods developed for experimenting at X-ray FELs and describe concepts for a sample environment that could facilitate automation in data collection, sample screening, and nozzle exchange, which may allow SFX experiments to be carried out at high efficiency.

II. SERIAL CRYSTALLOGRAPHY WITH PULSED SOURCES

The three guiding principles for SFX experiments listed above must necessarily be followed within the boundaries imposed by the characteristics of X-ray FEL sources and the limitations of instrumentation. Some relevant properties of current and pending X-ray FEL (XFEL) facilities are summarized in Table I. As is apparent from this table, the experimental conditions at sources with repetition rates of 120 Hz and lower are considerably different to the European XFEL, which delivers bursts of pulses at up to 4.5 MHz, and LCLS II, which is proposed to operate at 1 MHz for photon energies up to 5 keV. The pulse rate dictates the frame rate of detectors required for SFX as well as the required refresh speed of sample delivery. At LCLS and SACLA, the camera readouts match the pulse deliveries, with the Cornell-SLAC Pixel Array Detector (CSPAD; Hart *et al.*, 2012) and the Multi-Port Charge-Coupled Device (MPCCD; Kameshima *et al.*, 2014) optimized to record images at 120 Hz and 60 Hz, respectively. With the Adaptive Gain Integrating Pixel Detector (AGIPD; Becker and Graafsma, 2012), it will be possible to store 352 frames per

TABLE I. Principal properties to be considered for data collection, sample delivery, and characterization during SFX experiments at various hard X-ray FEL sources. The minimum sample speed is calculated assuming a required gap of 100 μm between pulses and assuming the source running at its highest-possible rate.

	LCLS	LCLS II (<5 keV)	SACLA	Swiss FEL	PAL XFEL	European XFEL
Pulse properties						
Pulses delivered per second	120	10^6	60	100	60	27 000
Highest pulse rate (Hz)	120	10^6	60	100	60	4.5×10^6
Shortest time between pulses	8.3 ms	1 μs	17 ms	10 ms	17 ms	220 ns
Detector properties						
Detector name	CSPAD	...	MPCCD	Jungfrau	MPCCD	AGIPD
Recordable image per seconds	120	...	60	100	60	3520
Veto option	No	...	No	Yes	No	Yes
Sample injection properties						
Required sample speed at maximum pulse rate	12 mm/s	100 m/s	6 mm/s	10 mm/s	6 mm/s	450 m/s

4.5 MHz European XFEL pulse train, providing a total of 3520 recorded frames per second. Although this is 10% of the maximum number of pulses that this facility can generate each second, a veto system implemented with the AGIPD may increase experiment efficiency.

Experimental methods that have been successfully developed at the low-rate facilities might not be transferrable to high-rate facilities without some modification or enhancement. However, experiments carried out so far provide crucial information on the interaction of X-ray pulses with samples and sample-carrying media and guide the development of the instrumentation required at future FEL sources. In particular, as mentioned above, an X-ray FEL pulse that is focused onto a frozen protein crystal destroys the structure in a region of about $25\text{ }\mu\text{m}$ diameter (Hirata *et al.*, 2014). Similarly, a length of destruction of about $100\text{ }\mu\text{m}$ was found in gas-focused liquid jets (Stan *et al.*, 2014), and hence any sample delivery system would need to move by at least this amount between X-ray pulses. Thus, it is clear that the optimum sample delivery method depends critically on the FEL repetition rate, and for a given repetition rate the sample must be delivered faster than the slowest required speed (shown in Table I) given by moving the sample by $100\text{ }\mu\text{m}$ between pulses. (Conversely, the repetition rate must be reduced for slower delivery systems. It will be possible to reduce the pulse rate at the European XFEL by arbitrarily filling the 2700 buckets within a pulse train, reducing the necessary speed of delivered samples.) Presumably, the destruction moves from the X-ray interaction point at the speed of sound, so it might be possible to take smaller steps if the delivery system moves faster than sound speed, which may be relevant for the 4.5 MHz pulse trains of the European XFEL. Since the X-ray exposure is set by the femtosecond pulse duration, samples would have to be moving at relativistic speeds before blurring during the exposure becomes an issue. However, unless the sample is delivered or arranged with a regular spacing (e.g., a pulsed jet) then the faster the delivery system, the more sample that is wasted between shots. We characterize the efficiency of the sample delivery as the fraction of delivered particles or crystals that are hit by a pulse and the hit fraction as the fraction of pulses that hit a particle.

The quantity of sample and the time required for a full measurement depend on how many patterns are necessary to generate a complete set of structure factors. In the Monte Carlo method, the relative standard error of the structure factors decreases as $1/\sqrt{N}$, where N is the number of patterns collected. The required signal to noise level depends on the phasing method, with molecular replacement requiring less than about a 20% convergence (quantified by the metric R_{split} ; White *et al.*, 2013). A survey of structures determined using FEL pulses, summarized in Table II and Figure 1, indicates that data quality varies considerably depending on the system, but for the most “well behaved” samples about 30 000 indexed patterns are required, giving a value of R_{split} of about 10%. As expected, collecting more patterns helps to improve data quality in proportion to the square root of the number of patterns (Figure 1). (Far fewer patterns are required when crystals are considerably bigger than the $25\text{ }\mu\text{m}$ zone of destruction, to allow rotation data to be collected, as discussed below.) Assuming a delivery system with a hit fraction of 10%, we then see that about 300 000 recorded frames are required for a full structure. This would take just over 40 min at the LCLS or 1.4 min at the European XFEL using the AGIPD without making use of the detector veto system. If the samples were delivered at a rate that matched the FEL pulse delivery, then the amount of material needed would be independent of that rate. The volume of the sample suspension under these ideal conditions could be estimated by assuming a medium of $3\text{ }\mu\text{m}$ diameter that moves $100\text{ }\mu\text{m}$ between shots, or a total volume of only $0.2\text{ }\mu\text{l}$ for a full data set. The 10% hit fraction could be achieved in the $3\text{ }\mu\text{m}$ thick delivery medium, and for a $1\text{ }\mu\text{m}^2$ focus and $1\text{ }\mu\text{m}^3$ crystals, at a crystal concentration of one crystal per $10 \times 3\text{ }\mu\text{m} \times 1\text{ }\mu\text{m}^2$ or $3 \times 10^{10}\text{ ml}^{-1}$, and a consumption of 0.5 pl per shot. The 300 000 frames would therefore require about $0.15\text{ }\mu\text{l}$ of suspension or about $6\text{ }\mu\text{g}$ of protein. However, we must stress that all delivery systems are far from this ideal, as discussed below and indicated in Table III.

III. SAMPLE DELIVERY TECHNOLOGIES FOR X-RAY FEL EXPERIMENTS

Here, we briefly summarize various systems for sample delivery developed for structural biology experiments at X-ray FEL sources. The list described below is not complete but

TABLE II. X-ray FEL structures deposited in the protein data bank (PDB) as of March 2015.

System	Residue	Patterns collected	Patterns indexed	R_{split}	PDB	References
SFX liquid						
Cathepsin B	240	3953 201	178 875	0.102	4HWY	Redecke 2013
Cry3A toxin	587	380 650	78 642	0.122	4QX0	Sawaya 2014
Cry3A toxin	587	380 688	76 308	0.159	4QX1	Sawaya 2014
Cry3A toxin	587	736 312	30 008	0.216	4QX2	Sawaya 2014
Cry3A toxin	587	736 360	30 952	0.244	4QX3	Sawaya 2014
Lysozyme	129	2402 199	59 667	0.061	4N5R	Barends 2014
Photosystem I	2334	1850 000	15 445	0.355	3PCQ	Chapman 2011
Reaction center	1192	365 035	265	...	4AC5	Johansson 2012
Reaction center	1212	2744 614	1175	0.365	4CAS	Johansson 2013
Photosystem II	5706	380 000	1850	...	4IXR	Kern 2013
Photosystem II	5706	2200 000	4663	...	4IXQ	Kern 2013
Photosystem II	5482	2 000 000	7269	...	4FBY	Kern 2012
Photosystem II	5276	...	34 554	0.070	4PBU	Kupitz 2014
Photosystem II	5276	...	18 772	0.090	4Q54	Kupitz 2014
Photosystem II	5674	703 720	10 924	...	4TNJ	Kern 2014
Photosystem II	5674	1 314 405	28 880	...	4TNI	Kern 2014
Photosystem II	5674	1 529 616	13 119	...	4TNH	Kern 2014
Photosystem II	5674	1 716 778	22 727	...	4TNK	Kern 2014
Photoactive Yellow Protein	125	207 168	64 496	0.065	4WL9	Tenboer 2014
Photoactive Yellow Protein	125	1 024 684	31 255	0.092	4WLA	Tenboer 2014
Thermolysin	316	651 793	11 455	0.244	4OW3	Hattne 2014
Thermolysin	316	757 546	125 800	...	4TNL	Kern 2014
SFX LCP/grease matrix						
FABP3	133	54 256	13 231	0.200	3WXQ	Sugahara 2015
Glucose isomerase	388	67 792	10 297	0.289	4W4Q	Sugahara 2015
Lysozyme	129	48 743	14 595	0.127	3WXT	Sugahara 2015
Lysozyme	129	86 305	29 323	0.077	3WXU	Sugahara 2015
Lysozyme	129	91 341	26 646	0.095	3WUM	Sugahara 2015
Lysozyme	129	101 330	34 438	0.087	3WUL	Sugahara 2015
Thaumatococcus	207	84 078	8856	0.164	3WXS	Sugahara 2015
5-HT2B serotonin receptor	430	4 217 508	32 819	0.095	4NC3	Liu 2013
Human smoothened receptor	468	3 510 525	61 964	0.098	4O9R	Weierstall 2014
δ -opioid receptor	832	1 967 539	36 083	0.118	4RWD	Fenalti 2015
FX fixed targets						
Cytochrome C	3614	1396	1107	0.243 ^a	3WG7	Hirata 2014
Myoglobin	154	932	739	...	4PNJ	Cohen 2014
Photosystem II	5384	5592	658	0.330 ^a	4UB6	Suga 2015
Photosystem II	5382	2058	680	0.294 ^a	4UB8	Suga 2015
Cytochrome C	3614	1396	1107	0.243 ^a	3WG7	Hirata 2014

^aValues of R_{merge} .

includes commonly used systems. The delivery technologies are summarized in Table III, except for the traditional in-air goniometer approach.

A. In-air goniometers

Goniometers used for macromolecular crystallography experiments at third generation synchrotrons were successfully adapted for X-ray FEL measurements, permitting data collection of large protein crystals with femtosecond pulses (Cohen *et al.*, 2014; Hirata *et al.*, 2014; and

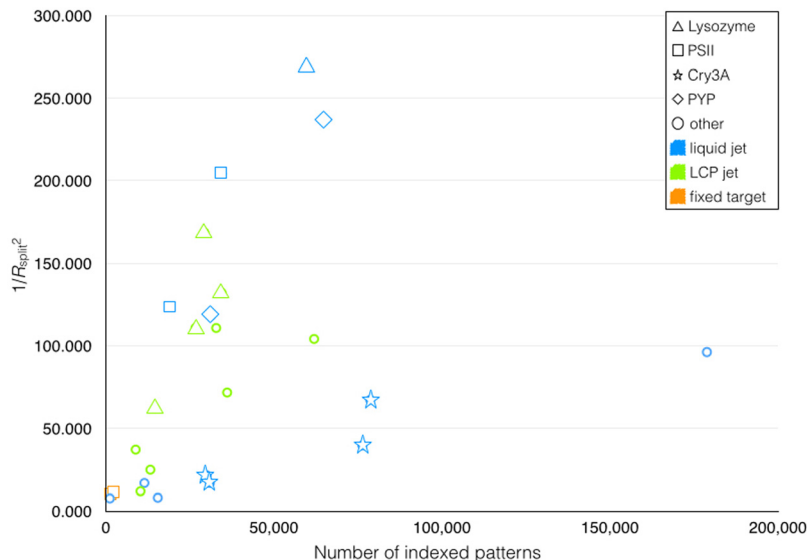


FIG. 1. Plot of $1/R_{\text{split}}^2$ versus the number of indexed patterns (see Table II). Blue, green, and orange colors represent data for liquid jets, LCP jets, and fixed targets, respectively. Multiple and independent data on similar proteins are highlighted by allocating symbols to these systems; Lysozyme data are associated with *triangles*, Photosystem II (PSII) with *squares*, Cry3A with *stars*, and PYP with *lozenges*. All the other data are represented by *circles*.

[Suga et al., 2015](#)). The goniometer and sample are in air, not vacuum, and at LCLS measurements have been carried out with a monochromatized beam. A diamond 111 monochromator typically selects 1% from the self-amplified spontaneous emission (SASE) spectrum ([Zhu et al., 2014](#)), reducing the pulse energy by this same factor. Nevertheless, when focused and unattenuated, the beam creates a region of destruction centered on the beam position. Crystals that are significantly larger than the damage diameter can be stepped to new positions and rotated between shots to acquire a rotation-step series from undamaged portions of the crystal and moving to new crystals after each is exhausted. The data can then be processed as if it was a set of conventional rotation series from multiple crystals. For example, [Hirata and colleagues \(2014\)](#) collected 1396 patterns from 76 crystals of Cytochrome C to obtain a structure from 40.0 to 1.9 Å resolution. Measurements can be carried out with single FEL pulses on demand, and automated crystal positioning has allowed measurements.

B. In-vacuum sample arrays

To facilitate room temperature studies of protein microcrystals only available in small quantities, [Hunter and colleagues \(2014\)](#) employed a silicon wafer with slotted openings with a

TABLE III. Suitable pulse repetition rates for various injection techniques. Pulse rate is calculated as fastest tolerable to ensure the sample moves by at least 100 μm between shots. At the European XFEL, there are 10 pulse trains per second. “Goniometer compatible” refers to whether the injector can be mounted on an in-vacuum goniometer.

Method	Sample phase	Speed (m/s)	Pulse rate (kHz)	Pulses per train	Pulsed	Goniometer compatible
GDVN	Liquid	3–30	300	180	Possibly	Yes
Electrospun jet	Liquid/polymer	1–30	300	180	Possibly	Yes
LCP extrusion	Viscous paste	0–0.1	1	1	Possibly	Yes
Aero-dynamic lens	Aerosol	5–20	200	120	Possibly	No
Aerosol nozzle	Aerosol	250	2500	1500	Possibly	Yes
Molecular beam	Gas	>1 000	10 000	2700	Yes	No
Membrane support	Solid or liquid	1	10	6	...	Yes (limited area)
Tape	Solid or liquid	10	100	60	...	No

200-nm thick silicon nitride membrane. The wafer membrane was coated with crystals and placed in the vacuum environment for collection of diffraction patterns using the focused LCLS unmonochromatized pulses. To prevent desiccation of the sample in the vacuum chamber, the crystals were removed from their buffer and resuspended in oil before this solution was painted onto the membranes. By continuously raster-scanning the wafer, SFX data could be recorded at 10 Hz and hit fractions above 38% could be achieved, which should allow a full dataset to be acquired with less than 1 mg of protein (Hunter *et al.*, 2014). The method is well suited for measuring diffraction from two-dimensional membrane crystals (Pedrini *et al.*, 2014) and is suitable for time-resolved measurements. Sample consumption could possibly be reduced further by using structured wafers where crystals become trapped in regularly spaced wells (Zarrine-Afsar *et al.*, 2012) or microfluidic chips (Heymann *et al.*, 2014). It should be possible to acquire data at 120 Hz if the array was moved at a speed greater than about 12 mm/s (see Table I) which perhaps could be performed without interruptions if the sample was only scanned in one direction, for example, as a thin tape (Roessler *et al.*, 2013).

C. Aerosol particle injectors

Single particle diffraction experiments with X-ray FEL pulses were envisioned to be carried out on particles in the gas phase, without any substrate or carrying medium that would create a background that may overwhelm the desired signal (Neutze *et al.*, 2000). Sample delivery technologies from mass spectroscopy were considered, and the first single-particle measurements at the Free-electron LASer in Hamburg (FLASH) were carried out using an aerodynamic lens (Bogan *et al.*, 2008). The aerosol is first created from the sample suspension at atmospheric pressure using a nebulizer such as an electrospray aerosol generator or a gas-focused liquid jet and introduced into the vacuum environment of the experiment through a series of skimmers, apertures, and pumping stages. The coaxial lens apertures tend to drive particles toward the central streamline by balancing particle inertial forces and drag forces. Lens stacks are thus optimized for a particular range of particle sizes, and for particles with diameters of about 100 nm, collimated beams of tens of microns can be achieved. The speed of the particles ranges from about 5 to 20 m/s. An aerodynamic lens was used for single-particle diffraction of virus particles (Seibert *et al.*, 2011), soot (Loh *et al.*, 2012), particle dimers (Starodub *et al.*, 2012), and cell organelles (Hantke *et al.*, 2014). High particle hit rates have been achieved, although the fraction of those hits that occur in the most intense part of the focused beam is lower. Thus, the hit fraction depends on the X-ray beam profile in the focus, which tends to have wide low-intensity wings, and the threshold at which a pattern is counted as a hit. It might be feasible to inject sub-micron sized crystals by this approach, which could benefit in collecting data with less background at lower energies.

Very recently, a compact aerosol injector was demonstrated that drives particles towards a focus of dimensions less than 10 μm diameter using a converging conical nozzle (Kirian *et al.*, 2015). The injector is comparable in size to the gas-focused liquid jets described below, and hence could be interchangeably mounted with those. This method utilizes only the one orifice and thus gas is emitted at high speed, imparting velocities to the particles above 250 m/s. The higher the particle speed, the lower the particle hit rate for a given X-ray pulse rate (since the particle density is reduced), but this injector is currently the only one with high enough speeds for the 4.5 MHz burst rate of the European XFEL.

D. Gas-focused liquid jets

The gas-focused dynamic virtual nozzle (GDVN) creates a jet of liquid that is typically a few microns in diameter moving at a velocity of several meters per second, injected into vacuum. Most SFX experiments to date have utilized GDVNs to deliver liquid suspensions of crystals to the beam. The nozzle consists of a hollow capillary usually made of glass and centered within a larger capillary tube. High-pressure gas flows through the interstitial space between the capillaries and focuses the liquid jet coming out of the inner capillary to a diameter that is much smaller than the orifice of that capillary (DePonte *et al.*, 2008). This avoids clogging of

the delivered particles that would occur by simply using a small orifice without gas focusing. Jet diameters of 1–5 μm are typically achieved, depending on the capillary diameters, the nozzle design, and the liquid and gas flows. Jet diameters as small as 300 nm have been demonstrated with a modified design where the orifice of the liquid line occurs at the point of the gas expansion into vacuum (DePonte *et al.*, 2009). The emitted liquid forms a cylindrical column that eventually breaks up into drops. The breakup can be driven at a fixed frequency so that droplets are timed to the X-ray pulse arrival (Shapiro *et al.*, 2008). However, since the drop diameter is about twice the column diameter, a lower background is achieved by placing the X-ray focus in the column. Particles and crystals that are elongated tend to align their long axis in the direction of the flow in the column and lose that alignment in the breakup region.

It has been the practice so far to run the jet continuously rather than pulsing it to match the X-ray repetition rate. As such, the liquid flow rate is typically greater than $10 \mu\text{l min}^{-1}$ and tens of milligrams of microcrystals are often required for a full data set. Photoactivated samples can be studied by laser-pumping the sample at the required time before the X-ray pulse arrival, which is usually done by illuminating the entire jet with the pump beam. However, for delays longer than about 100 μs , it may be necessary to illuminate the sample inside the nozzle (Kupitz *et al.*, 2014). By introducing another liquid capillary inserted in the first liquid line, it is possible to make a mixing jet (Wang *et al.*, 2014). Here, the sample can mix diffusively with a substrate in the laminar flow of the jet at a well-defined time before X-ray exposure, which can be varied by a clever telescopic design. GDVNs have also been made by applying the soft lithography techniques of microfluidics (Trebbin *et al.*, 2014). This has the advantage of easier mass production and in employing many designs for mixing and pulsing of jets.

E. Electrospun jets

Instead of gas focusing, electrospinning forms a small jet in vacuum or atmosphere by application of high voltage (between the liquid and an external electrode) that creates a Taylor cone. Samples can consist of particles embedded in a viscoelastic polymer or in a conductive liquid of the right viscosity (Sierra *et al.*, 2012 and Bogan *et al.*, 2008). Slower velocities than liquid jets can be attained, and voltage gives an extra degree of freedom that allows higher velocity for a given sample flow rate (producing sub-micron jets). Typical flow rates are 0.14 to $3.1 \mu\text{l min}^{-1}$. No effect of the high electric field on the sample has been observed in protein structures obtained using this delivery mechanism (Kern *et al.*, 2013). It is worth to note that this method is not suitable for measurements with synchrotron radiation since it was observed (in unpublished experiments at the Swiss Light Source by Bogan and Chapman) that the X-ray beam disrupts the formation of the Taylor cone, possibly due to ionization of the rest gas.

F. Extruded viscous flows

The LCP extrusion nozzle is similar to the GDVN except that the sample is embedded in a high-viscosity medium that is pushed out of a nozzle at high pressure (Weierstall *et al.*, 2014). This has primarily been used to dispense membrane proteins, such as G-protein coupled receptors, that crystallize in LCP (Liu *et al.*, 2013 and Weierstall, 2014). The diameter of the extruded material matches the nozzle diameter (about 20 to 50 μm). Coaxial gas is used to stabilize the flow direction, and the method works in vacuum or air (Botha *et al.*, 2015 and Nogly *et al.*, 2015). The velocity of the medium is much slower than that of liquid jets and can be varied between about 25 to 100 mm s^{-1} . This conserves sample and with the 120 Hz repetition rate of LCLS it has been possible to run the jet at less than 100 μm between shots, essentially hitting every crystal that flows by with an X-ray FEL repetition rate of 60 Hz. At the European XFEL, it would only be possible to utilize such jets with a single X-ray pulse per pulse train, that is, at 10 Hz. Due to the required high pressure, the reservoir must be located close to the nozzle, but the reservoir volume only needs be $<100 \mu\text{l}$.

A simpler extrusion injector, built from a syringe and without the gas stabilizing flow, was used to deliver soluble protein crystals embedded in a grease matrix with low sample consumption (Sugahara *et al.*, 2015). Although the sample consumption is greatly reduced by extrusion

as compared with liquid jets, the carrying medium is much thicker, producing proportionally more background, which may limit this approach to micron-sized crystals.

IV. TOWARDS AUTOMATION OF HIGH-THROUGHPUT SFX

As discussed above, high-rate FELs provide the potential to collect full datasets for a static structure in a much reduced time as compared with the low-rate facilities. Depending on the sample delivery method, this could also lead to a considerable reduction in sample consumption. The reduction in measurement time and required sample volume also opens up further opportunities for time-resolved studies, kinetics studies, fragment screening, and other multidimensional measurements where a parameter such as temperature or pH is varied. Given these possibilities and extrapolating from the high demand of beamtime at LCLS and SACLA, it is apparent that a system capable of high-throughput measurements is required. Here, high-throughput refers to being able to make many full and independent measurements per day (or shift) and requires a setup that is reliable and substantially automated.

Depending on the buffer and particle concentration, gas-focused liquid jet nozzles often have a limited lifetime in the beam before they need to be cleaned or replaced. Some causes of this are a build up of debris on the nozzle tip created by the X-ray induced sample explosion, formation of salt crystals on the exterior of the nozzle, or clogging of the capillary line (which is usually avoided with in-line filters). Another cause of down time is the growth of ice from a surface that the jet impacts back towards the nozzle. This occurs if the jet direction tilts towards a wall of the sample “catcher,” which may occur if the jet properties vary due to some of the external influences mentioned above. Using the current setups installed at LCLS or SACLA, manual exchange of the injector takes a few minutes for highly experienced users, added to the time required when performing nozzle and X-ray beam alignments as well as sample loading. Such a mode of operation is labor intensive, requiring people to perform the exchange and realignment and to prepare the replacement.

A higher efficiency could be achieved by robotic handling of the nozzle and implementing an automated alignment procedure. Moreover, a robotized nozzle exchange platform will enable quick sample changes, and automated alignment will allow closed-loop compensation of drifts of the jet position that are currently only corrected by hand. Such a system should be capable of handling the various types of injection methods discussed above that are likely to be used. One initial such prototype was constructed at the Centre for FEL Science (CFEL) and successfully used at LCLS and SACLA (Richard Bean, unpublished data). Briefly, the prototype consists of six placeholders where independent nozzles or other tools required during the

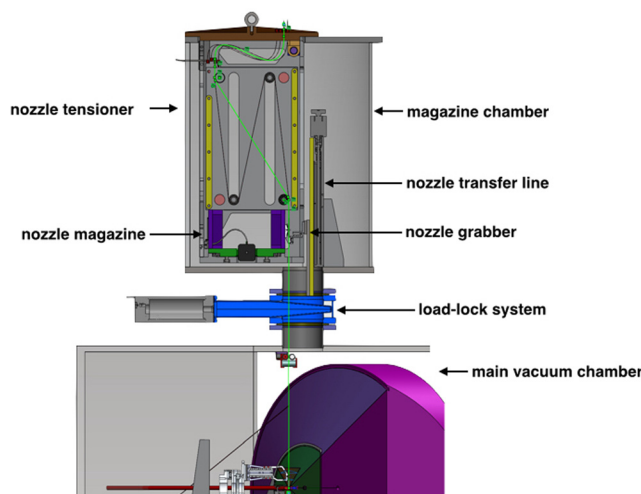


FIG. 2. Proposed design for a nozzle exchange system for automated SFX experiments. The *green* line corresponds to a pair of glass capillaries belonging to a GDVN injector when mounted at the interaction position.

experiments can be stored, ready to be mounted to the X-ray interaction region. Each nozzle can be independently mounted to the interaction point in less than 1 min, including alignment to the X-ray beam. The position of the inserted nozzle can be controlled by motorized stages with a precision of approximately 10 nm. The nozzle magazine is located close to the interaction region, which favors quick switching between nozzles but prevents any physical separation between the cartridge and the main vacuum chamber, which thus must be vented to replace the cartridge. This is compared with the Arizona State University nozzle rod system installed at the coherent X-ray imaging (CXI) instrument of LCLS (Weierstall *et al.*, 2012) that is inserted through a load-lock and hence permits manual nozzle exchange without breaking the vacuum of the sample chamber but requires external actuation to position the nozzle.

Building upon these ideas, we designed a prototype for high-throughput SFX that uses a 12-nozzle magazine mounted in a vacuum-tight compartment separated from the main sample

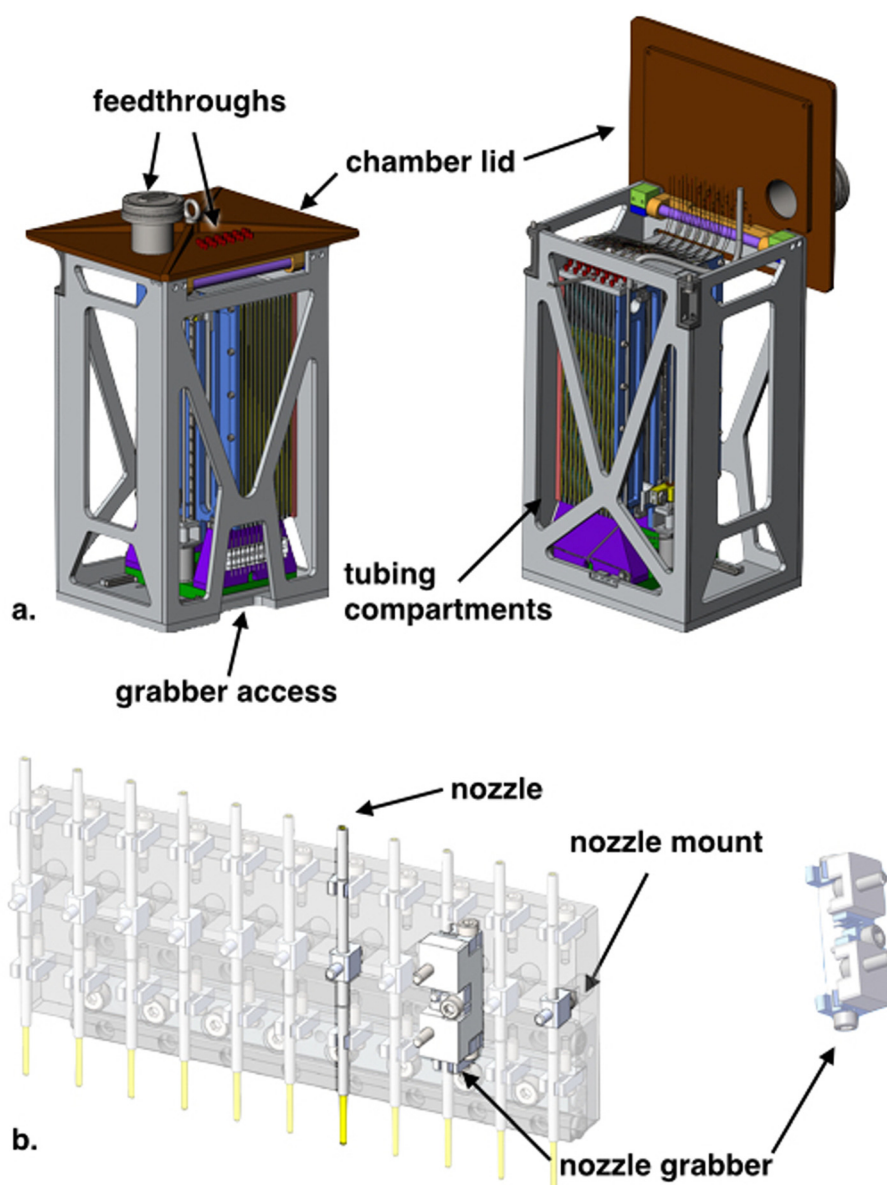


FIG. 3. (a) Nozzle tensioner with closed (*left*) and opened (*right*) lid. The nozzle magazine is represented in *purple*; tubing compartments are in *yellow*. (b) Nozzle magazine, with one nozzle highlighted, together with the nozzle mount and grabber system. The grabber is also shown from the opposite side, with nozzle mount clips illustrated in *blue*.

chamber by a load-lock system (Figure 2). Each nozzle can be mounted individually and exchanged by means of a nozzle grabber coupled to a nozzle transfer line that carries the injector through the load-lock system down to the main vacuum chamber and to the interaction region. Each pair of liquid and gas glass fibers for a given nozzle are contained within individual compartments of a tensioner that guides the fibers while being mounted or replaced in the cartridge (Figure 3(a)). The tensioner is part of the nozzle magazine and as such can be removed for pre-loading nozzles offline. The grabber system (Figure 3(b)) accommodates various sizes and designs of injectors, nozzles, or fixed targets through the use of a universal nozzle mount. This mount mates with the holders in the cartridge and the sample positioning system, and the transfer system. The sample positioning system is a state-of-the-art goniometer developed for synchrotron-based crystallography, which allows tilting the mounted injector in any direction within a cone of 30° half angle (Figure 4). Some samples tend to favor specific orientations in the flow of the jet, especially long needle-like crystals or fibers. By changing the orientation of the jet, it is possible to obtain complete coverage of structure factors, such as meridional reflections. In some cases, the jet direction can drift if salts or other materials build up over time near the nozzle tip. Arbitrary tilting of the nozzle allows maintaining a constant jet direction in these cases, which is required for closed-loop position control of the jet position. Care has been taken to prevent shadowing the diffraction camera.

SFX measurements are carried out in vacuum to avoid air scatter and the need for vacuum windows that also scatter and limit the beam intensity that can be used. The sample (e.g., liquid suspension) is injected into a “catcher” that is pumped with high speed and which maintains a low pressure in the main part of the sample chamber. The X-ray interaction takes place inside this catcher, which thus also prevents ejected debris from coating the main chamber, except in the direction of the detector which requires its own debris shield. The goniometer system then inserts the nozzle tip into an orifice at the top of the catcher, and the catcher position must therefore be adjustable so that it can be aligned to the X-ray beam that enters and exits through additional apertures in this structure. The exit window is conical in shape, allowing a scattering angle of 60° . Larger scattering angles could possibly be accommodated by raising the nozzle above the catcher or replacing the exit window of the catcher.

To maintain the jet in the beam and counteract drifts of the jet properties, we aim to implement active feedback of the jet position relative to the X-ray beam by real-time processing of a microscope image of the jet, to command the motorised nozzle positioner. This can be carried out using a microscope objective with a hole bored through its centre through which the incoming X-ray beam propagates, as has been used by us for coherent imaging experiments at FLASH. An additional camera orthogonal to the X-ray beam axis can be used to maintain the sample to detector distance. Both cameras are uncoupled from the nozzle manipulator, adding flexibility while operating the overall setup.

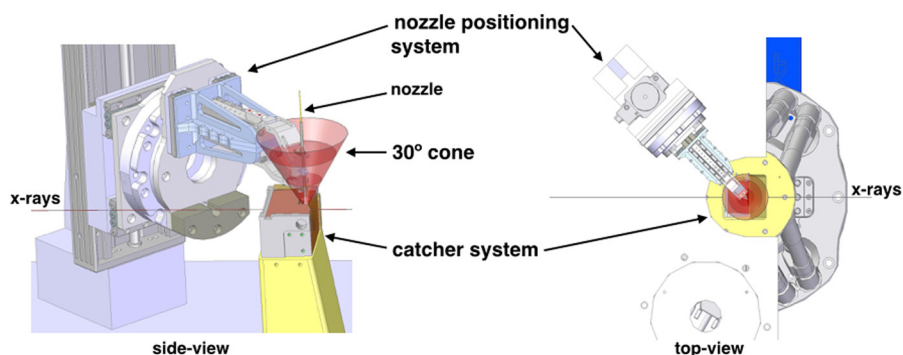


FIG. 4. Nozzle positioning system with nozzle mounted on the top of a catcher box. The goniometer is mounted at 45° from the X-ray axis. The *side-view* shows the tilting cone in red. The *top-view* shows the catcher (yellow) mounted on an hexapod (grey) and a load-lock gate valve (blue). The load-lock is used for cleaning the catcher system without having to break the main chamber vacuum. In these pictures, X-rays run from left to right.

V. CONCLUSIONS

X-ray FELs have offered a new way for structure determination, using femtosecond-duration pulses that allow room-temperature data collection from protein crystals at doses that are many orders of magnitude higher than possible by conventional techniques. The interaction with the focused X-ray pulse creates a zone of destruction in the sample of 50 to 100 μm in diameter. Thus for crystals smaller than this diameter, it is only possible to obtain a single still image per crystal. Serial crystallography aggregates data from tens of thousands of diffraction patterns measured from individual crystals to obtain a complete set of structure factors. Samples must be delivered to the X-ray beam at a rate that matches the pulse repetition rate of the source. In the case of the European XFEL operating at its maximum frequency of 4.5 MHz, this requires delivery speeds in excess of 450 m/s. Such a speed has only been approached so far with a gas nozzle (Kirian *et al.*, 2015), but it should be possible to somewhat increase the speed of liquid jets. Alternatively, the pulse repetition rate can be reduced to match the delivery speed (which may be required in any case to match the capability of the detector and X-ray optics). Although highest repetition rate and delivery speed certainly should give the shortest time to acquire a dataset, this is not necessarily the primary goal of any experimental design, which should prioritize obtaining the maximum diffraction data quality, especially on small or weakly diffracting crystals, and with samples of limited quantity or volume. There may be different sample delivery methods that will best achieve these goals for different sample properties or quantities, as we have reviewed here. While the field is still very young and new delivery methods are being developed, many of these methods use nozzles or sample holders of similar size, shape, or weight, and which can therefore be adopted for a universal sample holder. A compact goniometer system allows for a very flexible instrument for mounting such a range of devices and can be used as part of a highly automated measurement stage including stabilization of the jet by optical feedback and the robust exchange of nozzles through a vacuum load-lock. Such an automated approach could facilitate screening a large number of samples, each in a relatively short time, without requiring labor intensive procedures. This approach could also allow multidimensional measurements of samples over many conditions that are not currently feasible.

SFX is providing structures from samples at room temperature that may not be suitable for conventional methods, overcoming problems of radiation damage (especially for proteins with metal centers). However, the available X-ray FEL beamtime is considerably oversubscribed. The implementation of high throughput and automated systems for carrying out SFX experiments should therefore be of large benefit.

ACKNOWLEDGMENTS

The authors acknowledge Pegasus Design, Ltd. and SmarAct GmbH for their contributions to design and engineering. We also thank Kenneth Beyerlein, Holger Fleckenstein, Tokushi Sato, Carolin Seuring, Hamidreza Dadgostar, Uwe Weierstall, John Spence, and Petra Fromme for their input on the basic requirements for the sample injection and diagnostics setups, and we thank Sébastien Boutet (LCLS), Kensuke Tono (SACLA), Schertler Gebhard (SwissFEL), Jaehyun Park (PAL-FEL), Adrian Mancuso, Richard Bean (European XFEL), and Heinz Graafsma (DESY) for stimulating discussions. We acknowledge support from the serial femtosecond crystallography user consortium, funded by a joint Wellcome Trust - BBSRC award (WT102593MA), BMBF (05E13GU1, 05K13GU7, and 05K12GU3), the Swedish Research Council (VR), the Ministry of Education, Science, Research and Sport of the Slovak Republic, the Australian Research Council Centre of Excellence for Advanced Molecular Imaging (CE140100011), NSF Award No. STC 1231306, and DESY, a research centre of the Helmholtz Association.

Barends, T. R. M. *et al.*, “De novo protein crystal structure determination from X-ray free-electron laser data,” *Nature* **505**, 244–247 (2014).

Becker, J. and Graafsma, H., “Advantages of a logarithmic sampling scheme for XPCS experiments at the European XFEL using the AGIPD detector,” *J. Instrum.* **7**, P04012 (2012).

Bogan, M. J. *et al.*, “Single particle X-ray diffractive imaging,” *Nano Lett.* **8**, 310–316 (2008).

- Botha, S. *et al.*, "Room-temperature serial crystallography at synchrotron X-ray sources using slowly flowing free-standing high-viscosity microstreams," *Acta Crystallogr., Sect. D: Biol. Crystallogr.* **71**, 387–397 (2015).
- Boutet, S. *et al.*, "High-resolution protein structure determination by serial femtosecond crystallography," *Science* **337**, 362–364 (2012).
- Chapman, H. N. *et al.*, "Femtosecond X-ray protein nanocrystallography," *Nature* **470**, 73–77 (2011).
- Cohen, S. *et al.*, "Goniometer-based femtosecond crystallography with X-ray free electron lasers," *Proc. Natl. Acad. Sci. U. S. A.* **111**, 17122–17127 (2014).
- DePonte, D. P. *et al.*, "Gas dynamic virtual nozzle for generation of microscopic droplet streams," *J. Phys. D: Appl. Phys.* **41**, 195505 (2008).
- DePonte, D. P. *et al.*, "SEM imaging of liquid jets," *Micron* **40**, 507–509 (2009).
- Fenalti, G. *et al.*, "Structural basis for bifunctional peptide recognition at human δ -opioid receptor," *Nat. Struct. Mol. Biol.* **22**, 265–268 (2015).
- Hantke, M. F. *et al.*, "High-throughput imaging of heterogeneous cell organelles with an X-ray laser," *Nat. Photonics* **8**, 943–949 (2014).
- Hart, P. *et al.*, "The CSPAD megapixel X-ray camera at LCLS," *Proc. SPIE* **8504**, 85040C (2012).
- Hattne, J. *et al.*, "Thermolysin structure determined by free-electron laser," *Nat. Methods* **11**, 545–548 (2014).
- Henderson, R., "Cryo-protection of protein crystals against radiation damage in electron and X-ray diffraction," *Proc. R. Soc. London, Ser. B* **241**, 6–8 (1990).
- Heymann, M. *et al.*, "Room-temperature serial crystallography using a kinetically optimized microfluidic device for protein crystallization and on-chip X-ray diffraction," *IUCrJ* **1**, 349–360 (2014).
- Hirata, K. *et al.*, "Determination of damage-free crystal structure of an X-ray-sensitive protein using an X-ray FEL," *Nat. Methods* **11**, 734–736 (2014).
- Hunter, M. S. *et al.*, "Fixed-target protein serial microcrystallography with an X-ray free electron laser," *Sci. Rep.* **4**, 6026 (2014).
- Johansson, L. C. *et al.*, "Lipidic phase membrane protein serial femtosecond crystallography," *Nat. Methods* **9**, 263–265 (2012).
- Johansson, L. C. *et al.*, "Structure of a photosynthetic reaction centre determined by serial femtosecond crystallography," *Nat. Commun.* **4**, 2911 (2013).
- Kameshima, T. *et al.*, "Development of an X-ray pixel detector with multi-port charge-coupled device for X-ray free-electron laser experiments," *Rev. Sci. Instrum.* **85**, 033110 (2014).
- Kern, J. *et al.*, "Room temperature femtosecond X-ray diffraction of photosystem II microcrystals," *Proc. Natl. Acad. Sci. U. S. A.* **109**, 9721–9726 (2012).
- Kern, J. *et al.*, "Simultaneous femtosecond X-ray spectroscopy and diffraction of photosystem II at room temperature," *Science* **340**, 491–495 (2013).
- Kern, J. *et al.*, "Taking snapshots of photosynthetic water oxidation using femtosecond X-ray diffraction and spectroscopy," *Nat. Commun.* **5**, 4371 (2014).
- Kirian, R. A. *et al.*, "Structure-factor analysis of femtosecond microdiffraction patterns from protein nanocrystals," *Acta Crystallogr., Sect. A: Found. Crystallogr.* **67**, 131–140 (2011).
- Kirian, R. A. *et al.*, "Simple convergent-nozzle aerosol injector for single-particle diffractive imaging with x-ray free-electron lasers," *Struct. Dyn.* (to be published) (2015).
- Kupitz, C. *et al.*, "Serial time-resolved crystallography of photosystem II using a femtosecond X-ray laser," *Nature* **513**, 261–265 (2014).
- Liu, P., Ziemann, P. J., Kittelson, D. B., and McMurry, P. H., "Generating particle beams of controlled dimensions and divergence: I. Theory of particle motion in aerodynamic lenses and nozzle expansions," *Aerosol Sci. Technol.* **22**, 293–313 (1995).
- Liu, W. *et al.*, "Serial femtosecond crystallography of G protein-coupled receptors," *Science* **342**, 1521–1524 (2013).
- Loh, N. D. *et al.*, "Fractal morphology, imaging and mass spectrometry of single aerosol particles in flight," *Nature* **486**, 513–517 (2012).
- Neutze, R. *et al.*, "Potential for biomolecular imaging with femtosecond X-ray pulses," *Nature* **406**, 752–757 (2000).
- Nogly, P. *et al.*, "Lipidic cubic phase serial millisecond crystallography using synchrotron radiation," *IUCrJ* **2**, 168–176 (2015).
- Owen, R. L., Rudino-Pinera, E., and Garman, E. F., "Experimental determination of the radiation dose limit for cryocooled protein crystals," *Proc. Natl. Acad. Sci. U.S.A.* **103**, 4912–4917 (2006).
- Pedrin, B. *et al.*, "7 Å resolution in protein two-dimensional-crystal X-ray diffraction at Linac Coherent Light Source," *Philos. Trans. R. Soc. London, Ser. B* **369**, 20130500 (2014).
- Redecke, L. *et al.*, "Native inhibited Trypanosoma brucei cathepsin B structure determined by using an X-ray laser," *Science* **339**, 227–230 (2013).
- Roessler, C. G. *et al.*, "Acoustic methods for high-throughput protein crystal mounting at next-generation macromolecular crystallographic beamlines," *J. Synchrotron Radiat.* **20**, 805–808 (2013).
- Sawaya, M. R. *et al.*, "Protein crystal structure obtained at 2.9 Å resolution from injecting bacterial cells into an X-ray free-electron laser beam," *Proc. Natl. Acad. Sci. U.S.A.* **111**, 12769–12774 (2014).
- Seibert, M. M. *et al.*, "Single mimivirus particles intercepted and imaged with an X-ray laser," *Nature* **470**, 78–81 (2011).
- Shapiro, D. *et al.*, "Powder diffraction from a continuous microjet of submicrometer protein crystals," *J. Synchrotron Radiat.* **15**, 593–599 (2008).
- Sierra, R. G. *et al.*, "Nanoflow electrospinning serial femtosecond crystallography," *Acta Crystallogr., Sect. D: Biol. Crystallogr.* **68**, 1584–1587 (2012).
- Spence, J. C. and Chapman, H. N., "The birth of a new field," *Philos. Trans R. Soc. London, Ser. B* **369**, 20130309 (2014).
- Stan, C. *et al.*, "The fluid dynamics of microjet explosions caused by extremely intense X-ray pulses," 2014, see <http://meetings.aps.org/Meeting/DFD14/Session/G10.10>.
- Starodub, D. *et al.*, "Single-particle structure determination by correlations of snapshot X-ray diffraction patterns," *Nat. Commun.* **3**, 1276 (2012).

- Suga, M. *et al.*, "Native structure of photosystem II at 1.95 Å resolution viewed by femtosecond X-ray pulses," *Nature* **517**, 99–103 (2015).
- Sugahara, M. *et al.*, "Grease matrix as a versatile carrier of proteins for serial crystallography," *Nat. Methods* **12**, 61–63 (2015).
- Tenboer, J. *et al.*, "Time-resolved serial crystallography captures high-resolution intermediates of photoactive yellow protein," *Science* **346**, 1242–1246 (2014).
- Trebbin, M. *et al.*, "Microfluidic liquid jet system with compatibility for atmospheric and high-vacuum conditions," *Lab Chip* **14**, 1733–1745 (2014).
- van der Schot, H. *et al.*, "Imaging single cells in a beam of live cyanobacteria with an X-ray laser," *Nat. Commun.* **6**, 5704 (2015).
- Wang, D., Weierstall, U., Pollack, L., and Spence, J., "Double-focusing mixing jet for X-ray FEL study of chemical kinetics," *J. Synchrotron Radiat.* **21**, 1364–1366 (2014).
- Weierstall, U., "Liquid sample delivery techniques for serial femtosecond crystallography," *Philos. Trans. R. Soc. London, Ser. B* **369**, 20130337 (2014).
- Weierstall, U., Spence, J. C., and Doak, R. B., "Injector for scattering measurements on fully solvated biospecies," *Rev. Sci. Instrum.* **83**, 035108 (2012).
- Weierstall, U. *et al.*, "Lipidic cubic phase injector facilitates membrane protein serial femtosecond crystallography," *Nat. Commun.* **5**, 3309 (2014).
- White, T. A. *et al.*, "CrystFEL: A software suite for snapshot serial crystallography," *J. Appl. Cryst.* **45**, 335–341 (2012).
- White, T. A. *et al.*, "Crystallographic data processing for free-electron laser sources," *Acta Crystallogr., Sect. D: Biol. Crystallogr.* **69**, 1231–1240 (2013).
- Zarrine-Afsar, A. *et al.*, "Crystallography on a chip," *Acta Crystallogr., Sect. D: Biol. Crystallogr.* **68**, 321–323 (2012).
- Zhu, D. *et al.*, "Performance of a beam-multiplexing diamond crystal monochromator at the Linac Coherent Light Source," *Rev. Sci. Instrum.* **85**, 063106 (2014).